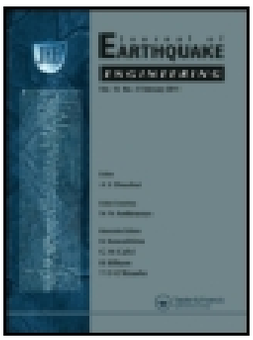

Journal of Earthquake Engineering

ISSN: 1363-2469 (Print) 1559-808X (Online) Journal homepage: https://www.tandfonline.com/loi/ueqe20

The Mw 6.4 SW-Achaia (Western Greece) Earthquake of 8 June 2008: Seismological, Field, GPS Observations, and Stress Modeling

A. Ganas , E. Serpelloni , G. Drakatos , M. Kolligri , I. Adamis , Ch. Tsimi & E. Batsi

To cite this article: A. Ganas , E. Serpelloni , G. Drakatos , M. Kolligri , I. Adamis , Ch. Tsimi & E. Batsi (2009) The Mw 6.4 SW-Achaia (Western Greece) Earthquake of 8 June 2008: Seismological, Field, GPS Observations, and Stress Modeling, Journal of Earthquake Engineering, 13:8, 1101-1124, DOI: 10.1080/13632460902933899

To link to this article: https://doi.org/10.1080/13632460902933899

Journal of Earthquake Engineering, 13:1101–1124, 2009

ISSN: 1363-2469 print / 1559-808X online
DOI: 10.1080/13632460902933899

Taylor & Francis
Taylor & Francis Group

The Mw 6.4 SW-Achaia (Western Greece) Earthquake of 8 June 2008: Seismological, Field, GPS Observations, and Stress Modeling

A. GANAS[1], E. SERPELLONI[2], G. DRAKATOS[1], M. KOLLIGRI[1], I. ADAMIS[1], CH. TSIMI[1], and E. BATSI[1]

[1]Institute of Geodynamics, National Observatory of Athens, Athens, Greece
[2]Istituto Nazionale di Geofisica e Vulcanologia, Centro Nazionale Terremoti, Bologna, Italy

On June 8, 2008 a Mw = 6.4 earthquake occurred in NW Peloponnese, western Greece. This event is the largest strike-slip earthquake to occur in western Greece during the past 25 years. No surface rupture was observed. Many rock falls, slides, and liquefaction features have been found as is typical for an earthquake of this size. Double-difference relocations of 370 aftershocks show a linear pattern of events and define a clear NE-SW striking mainshock fault plane. The hypocentrer was determined at 18 km depth beneath village Mihoi in SW Achaia. The 24-hr aftershock region extends approximately 30 km in length, and the width of the surface projection of the aftershocks ranges between 5–10 km. The depth of the aftershocks rarely exceeds 22 km. Analysis of high-rate GPS data showed that station RLS (Riolos) which is located 12.8 km N5°W of the epicenter was displaced co-seismically 7 mm to the North in agreement with right-lateral kinematics of the rupture. Static (Coulomb) stress transfer analysis indicates loading of faults near the towns of Patras (north) and Amaliada (south), respectively. The earthquake put more emphasis on the role of strike-slip in the deformation of western Greece also indicating that seismic strain is partitioned between strike-slip and normal-slip events due to obliquity of the Nubia (Africa) – Eurasia convergence.

Keywords Western Greece; Strike-Slip; Seismicity; GPS; HypoDD; Coulomb Stress; Active Tectonics

1. Introduction

The location of the June 8, 2008 epicentral area is in NW Peloponnese (western Greece; Fig. 1) near the western termination of the Hellenic Arc. This is a region of diverse topography ranging from a gently sloping land in the west, to a mountainous area in the east. The area is located between the Gulf of Corinth extensional province [Ambraseys and Jackson, 1997] and the Eurasia-Africa plate boundary offshore Cephalonia and Zakynthos Islands. In NW Peloponnese the instrumental seismicity records and general knowledge of active structures indicate that faults are relatively small but sufficient to generate earthquakes with $5.0 < M < 5.8$ [Table 1; Galanopoulos, 1981; Tselentis *et al*., 1994; Melis *et al*., 1994; Kiratzi and Louvari, 2003].

According to the fault plane solutions determined from various institutes, the June 8, 2008 earthquake ruptured a nearly vertical, strike-slip fault (see compilation in Table 2).

Received 20 September 2008; accepted 23 March 2009.

Address correspondence to A. Ganas, Institute of Geodynamics, National Observatory of Athens, Lofos Nymfon, Thission, Athens 118 10, Greece; E-mail: aganas@gein.noa.gr

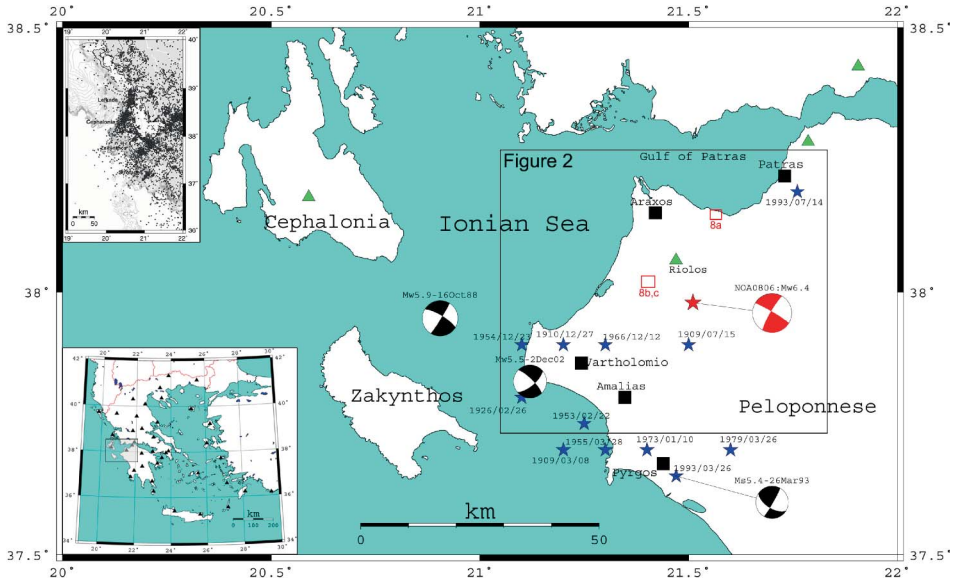

FIGURE 1 Map of the study area showing important towns, the June 8, 2008 epicenter (red star) and past events (blue stars). Green triangles indicate locations of seismic stations close to epicenter. Red boxes indicate field localities described on Figure 8. Beachballs indicate focal mechanisms of strike-slip events (shaded quadrants are compressional). Inset box upper left: seismicity map from [Roumelioti *et al.*, 2007]. Inset box lower left: map of Greece indicating study area. Black triangles in inset box show locations of permanent, three-component seismic stations in Greece. (Figure available in color online.)

TABLE 1 Past seismicity: events for the period 1909–1979 are from Galanopoulos, [1981; MAG is Ms], events after 1979 are from the NOA on-line catalogue (www.gein.noa.gr; MAG is ML). This combined catalogue is complete up to M = 5.5 since 1909 and up to M = 4.8 since 1953. The intensities are given by Galanopoulos

Date (yyyy/mm/dd)	Lat	Lon	MAG	Meisoseismal town
1909/03/08	37.70	21.20	5.5	Katakolon
1909/07/15	37.90	21.50	5.7–5.8	Chavari
1910/12/27	37.90	21.20	5.7–5.8	Vartholomio
1926/02/26	37.80	21.10	5.5	Kyllene
1953/02/22	37.70	21.20	4.8–5	Kyllene VIII
1954/12/23	37.90	21.20	6	Vartholomio VIII
1955/03/28	37.70	21.20	5.7–5.8	Gastouni VIII
1966/12/12	37.90	21.30	4.8–5	Savalia VII
1973/01/10	37.70	21.40	5.7–5.8	Kollyrion VIII
1979/03/26	37.70	21.60	5.2–5.3	Varvasaina VII
1988/10/16	37.90	20.96	5.5	Kyllene
1993/03/26	37.65	21.44	5.0	Pyrgos
1993/07/14	38.16	21.76	5.1	Saravalli
2002/12/02	37.80	21.15	5.3	Vartholomio
2008/06/08	37.98	21.51	6.5	Mihoi

TABLE 2 Summary of June 8, 2008, 12:25 UTC parameters as determined by various seismological institutes around the world. [1]NOA Moment Tensor solution is reported at: http://bbnet.gein.noa.gr/mt_solution/20080608_122530.NOA_IG_MT.html [2]NOA catalogue location is reported at: http://194.177.194.200/services/monthly-list.html [3]The CMT catalog search is available at: http://www.globalcmt.org/CMTsearch.html [4]The MEDNET solution can be retrieved from: http://mednet.rm.ingv.it/rcmt.php [5]The Swiss solution is available from http://www.seismo.ethz.ch/mt/armt/full_armt.html [6]AUTH and USGS solutions were taken from the special CSEM web page http://www.emsc-csem.org P- and T-axis are given as plunge/azimuth, respectively. The azimuth of the P-axis ranges between N59°E – N76°E while the plunge is near-horizontal

Institute	Lat	Long	Strike	Dip	Rake	P-axis	T-axis	DEPTH	MAG	Scalar Moment
NOA_MT[1,2]	37.98	21.48	210	82	175	2/75		22	Mw = 6.4	4.49×10^{25} (dyn cm)
Global CMT Catalog[3]	37.97	21.60	210	86	162			15	Mw = 6.3 mb = 6.1 Ms = 6.1	3.89×10^{25}
Mednet-RCMT[4]	37.99	21.52	210	85	179	3/75	4/166	38	ML = 6.2 Mw = 6.5	6.00×10^{25}
SWISS (ETHZ)[5]	38.01	21.44	213	81	165	4/259	15/168	31	Mw = 6.4	5.71×10^{25}
CSEM	37.968	21.483	–	–	–			5	Mw = 6.4	–
AUTH[6]	37.97	21.50	211	90	178			30	Mw = 6.5	6.50×10^{25}
PATRA[6]	–	–	–	–	–			–	–	–
USGS[6]	38.146	21.593	30	89	−160	13/256	12/163	10	Mw = 6.3	3.1×10^{18} (N m) 3.1×10^{25} (dyn cm)

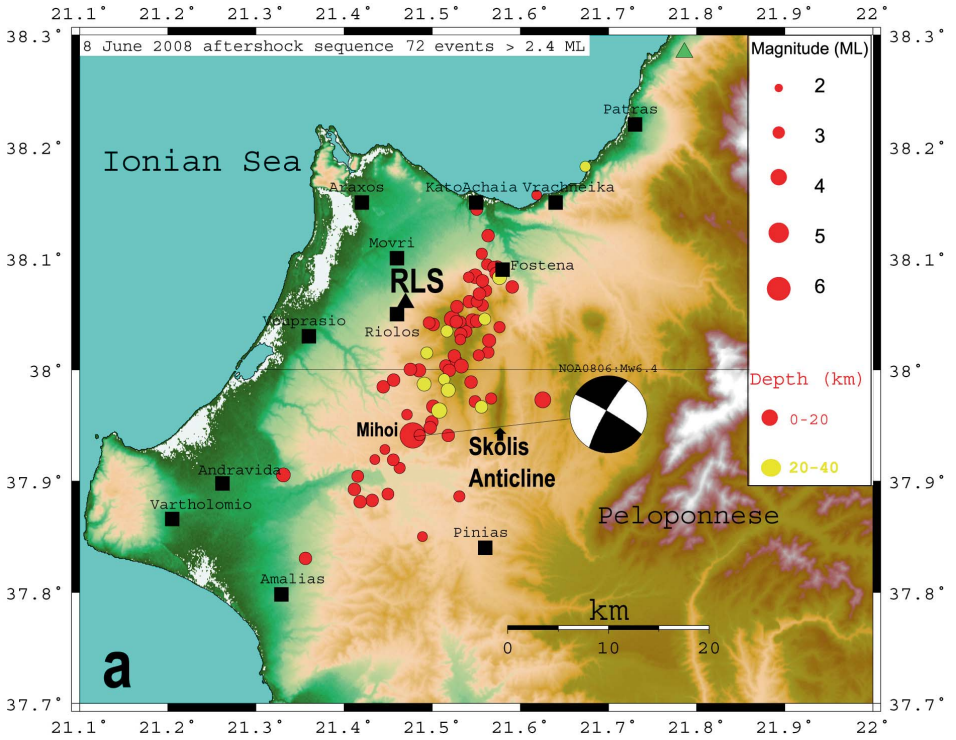

FIGURE 2 Relief map of southwestern Achaia and Northern Elis (Peloponnese, Greece) showing mainshock epicenter and relocated aftershocks from NOA network. a) 72 well-located events with 2.4 < ML < 4.2 during the first 24 h. Their alignment defines a NE-SW striking fault plane (b) 370 well-located events with 2.1 < ML < 4.4 have been determined during the period June 8–July 11, 2008 (approximately one month). Cyan solid line indicates inferred location of seismic fault (without surface expression). Arrows indicate sense of motion of crustal blocks. Black squares are urban centers. Beachball indicates NOA focal plane solution of the mainshock (lower hemisphere projection, compressional quadrants are black). (Figure available in color online.)

This fault is located beneath the mountains Movri and Skolis in southwest Achaia province and caused damage in the provinces of Achaia and Elis (western Greece; Fig. 2). Such types of earthquakes are not uncommon in western Greece and are due to a compressional component of the differential motion between the Nubia (Africa) and Aegean (Eurasia) plates [Benetatos *et al.*, 2004]. Recent strike-slip events in this area include the offshore events of Kyllene earthquake in October 16, 1988 [M_L = 5.5; Lekkas *et al.*, 1991; Fig. 1] and of Vartholomio earthquake in December 2, 2002 [M = 5.5; Roumelioti *et al.*, 2004]. Those events were located about 30–40 km to the W–WSW of the June 8, 2008 event. For the onshore area a recent relocation study combining phases from all three available earthquake catalogs in Greece for the period 2000–2005 showed scarce seismicity [Fig. 1, inset; Roumelioti *et al.*, 2007].

The June 8, 2008 M = 6.4 event came as a surprise due to both its magnitude and lack of surface faulting. In this article, we report on several aspects of the earthquake including distribution and focal mechanisms of aftershocks, static stress transfer effects,

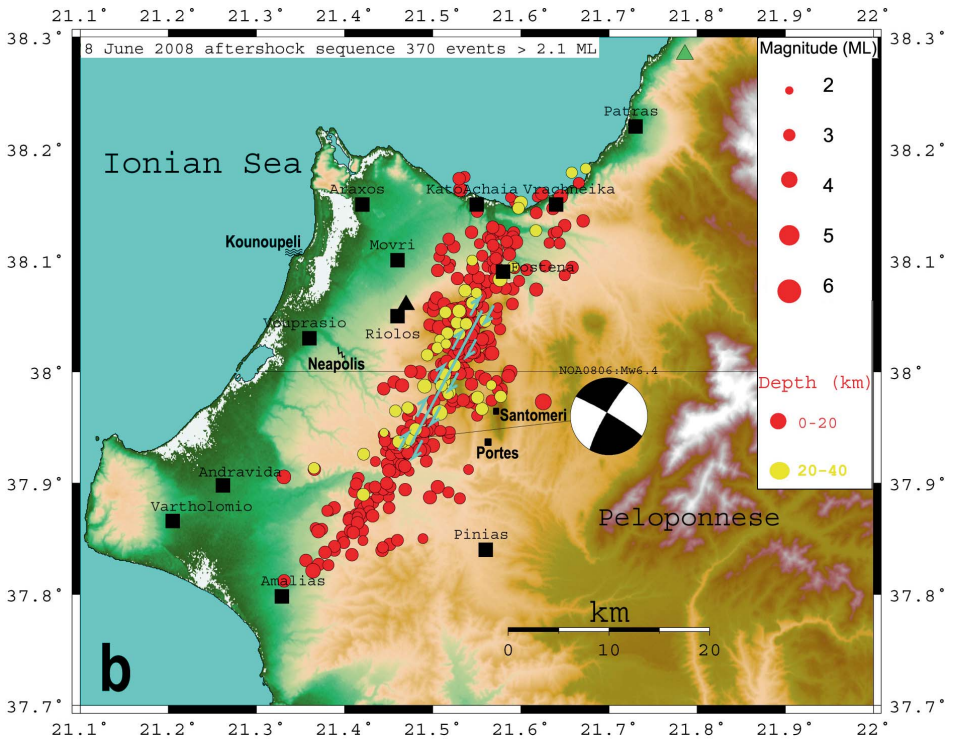

FIGURE 2 (*Continued*).

surface effects, and GPS observations. We also discuss the implications of this strike-slip event for the regional tectonics and the origin of the coastal uplift.

2. Geological Setting

South Achaia and Northern Ellis provinces of NW Peloponnese (western Greece) are characterized by a pile of N–S striking carbonate nappes separated from one another by major west-verging thrust faults. These nappes include the Pindos, the Gavrovo-Tripolitza, and the Ionian zones. Each nappe consists of a Mesozoic to early Tertiary pelagic (Ionian and Pindos) and neritic (Gavrovo) sediments, overlain by a clastic sequence of clays and turbiditic sandstones (flysch) that accumulated during nappe stacking in front of the active nappe-bounding thrust. The progressively younger ages of the flysch units from E to W reflect the westward propagation of nappe stacking which terminated in Miocene times. The main structure near the epicenter is the Skolis anticline (Fig. 2) which is made by Gavrovo carbonates thrusted onto the Tertiary flysch of the Ionian zone. Post-orogenic extension begun during the Upper Pliocene with formation of Elis and Pyrgos basins to the south and Gulf of Patras to the north [Ferentinos *et al.*, 1985; Doutsos *et al.*, 1987, 1988]. The Plio-Quaternary deposits are of shallow marine and lagoonal facies and reach a maximum thickness of 1500 m [Kamberis *et al.*, 1992]. Current extension direction is north-south [Hollestein *et al.*, 2008]. During Late

Quaternary the area underwent uplift as demonstrated by dating of uplifted marine terraces [Stamatopoulos *et al.*, 1988].

3. Seismological Data Analysis

On June 8, 2008 at 12:25 UTC (15:25 local summer time), a strong earthquake (NOA Mw = 6.4; Global CMT (Centroid Moment Tensor) Mw = 6.3, USGS Mw = 6.3; Table 2) occurred in SW-Achaia (Fig. 2) of western Greece. The NOA MT solution has a Misfit = 0.23, CLVD (Compensated Linear Vector Dipole) = 4.2% and depth = 22 km. However, similar solutions with misfit values < 0.25 are obtained for depths in the range 15–25 km and slightly higher CLVD values (∼10%). The earthquake occurred, in a region where the principal compressional stress axis lies horizontally E-W or ENE-WSW (see P-axis azimuth in Table 2). The strike-slip-type source was determined by broadband waveforms recorded by the NOA Digital Seismic Network (Figure 3; http://bbnet.gein.noa.gr/; see Melis and Konstantinou [2006] for procedures). As there was no surface rupture the seismic fault was determined from the NE-SW alignment of aftershocks (Fig. 2). Based on the finite fault model (see later in this article), we calculated that the NE-striking fault plane slipped up to about 73 cm during the mainshock. The fault dip direction was determined to the NW by most institutes (Table 2) at a steep angle. Using Hypo-DD relocation and the local 1-D velocity model by Haslinger *et al*. (1999; Table 3) we determined the focal depth at 18 km (see section to follow for details). The mid-crustal depth of this event was not unexpected as the depth of 20–25 km is thought to be the lower limit of the seismogenic zone in NW Peloponnese (Moho is located at about 40 km) [Sachpazi *et al.*, 2007]. The 2002 strike-slip event offshore Vartholomio (Fig. 1) occurred at a depth of 17 km [Roumelioti *et al.*, 2004]. Also, the 1993 Patras earthquake aftershocks reached depths of 20–30 km [Melis *et al.*, 1994]. The data of Hatzfeld *et al.* [1990] show events with depths ranging from 0–40 km. In addition, the 18 km depth of the earthquake source was responsible for the absence of primary seismic ruptures in the field.

To determine aftershock hypocenters, event phases were subsequently passed to HypoDD code (a FORTRAN program) that implements the double-difference earthquake location algorithm of Waldhauser and Ellsworth [2000] and Waldhauser [2001]. We used data from proximal (epicentral distance < 200 km) Greek stations collected at the acquisition server of NOA (Fig. 3a; a list of stations can be found at: http://bbnet.gein.noa.gr/QC/htdocs/index.html). Earthquake relocation with hypoDD is a two-step process. The first step involves the analysis of phase data to derive travel time differences for pairs of earthquakes. In the second step, the differential travel time data from step one is used to determine double-difference hypocenter locations. HypoDD run several times to test different 1-D velocity models (Table 3) and different P- and S-phases weighting schemes. The [Haslinger *et al.*, 1999] 1-D velocity model for the Gulf of Arta (western Greece) and a ratio Vp/Vs = 1.78 was finally used. The choice of the 1-D optimum velocity model was made on the following criteria: (a) the overall better statistics (the RMS of the solution per each station used is given in Table 4) and (b) the calculation of shallower depths of the aftershock sequence (Fig. 4d). The use of the NOA 1-D model (Table 3) provided a mean depth of the aftershocks equal to 21.2 km, while the Patras model (as reported by Roumelioti *et al.*, 2007) and the Haslinger *et al.* [1999] model equal to 19.9 and 16.4 km, respectively (see Fig. 4d for a detailed comparison). The Haslinger *et al.* [1999] velocity model provided shallower events which seemed to us more realistic in view of the expected thickness of the seismogenic part of the crust. During HypoDD procedure linked events were weighted and the following weights were applied: WTCTP (a-priori

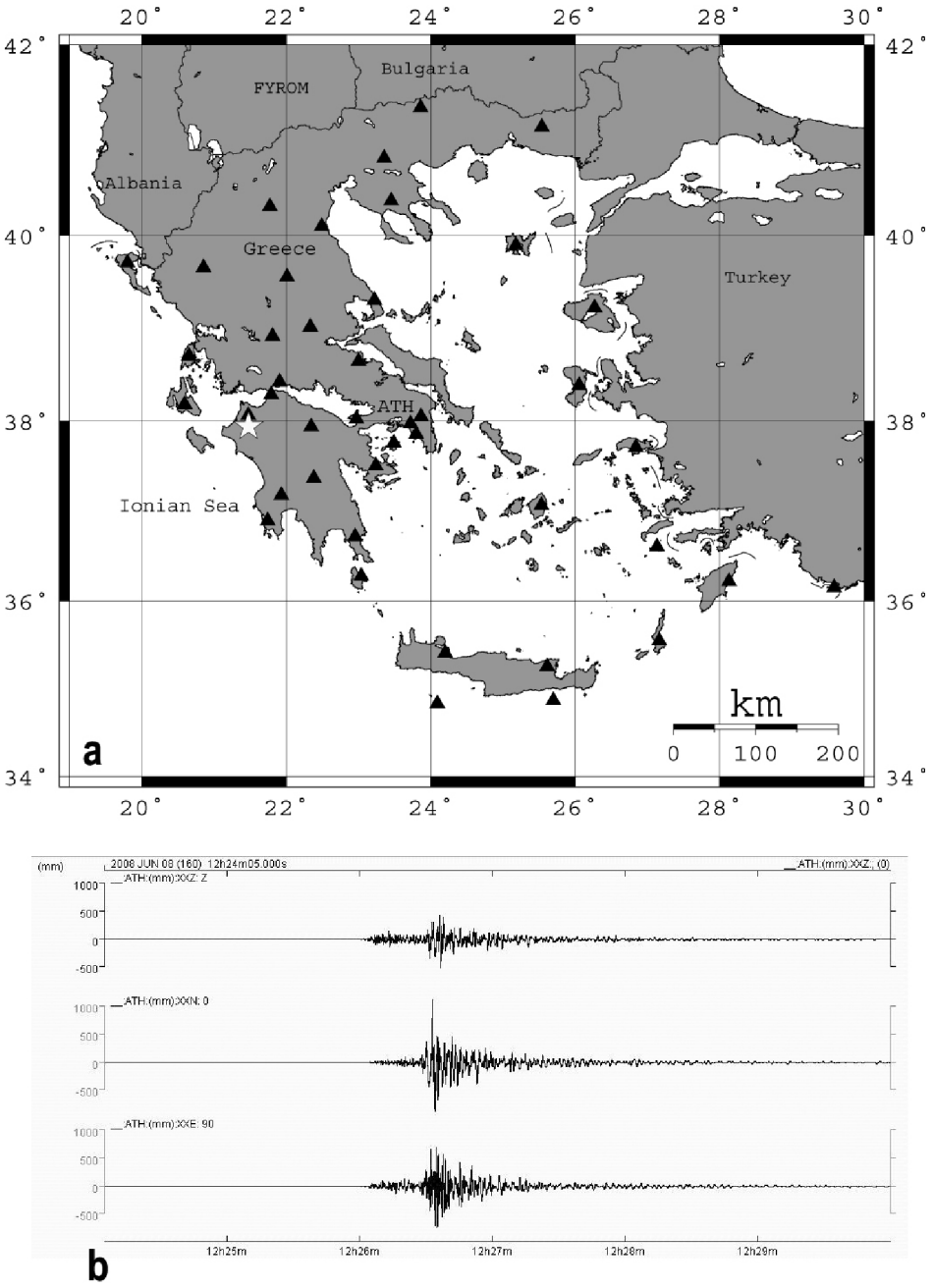

FIGURE 3 (a) Map of Greek stations which recorded the mainshock. Stations are shown as solid triangles and the June 8, 2008 epicenter by a white star. (b) The displacement –filtered waveforms of the June 8, 2008 earthquake recorded at the Athens station (ATH in Fig. 3a). Epicentral distance is 193 km. Y-axis units in mm.

TABLE 3 The 1-D velocity models used in aftershock relocation. The Athens and Patras 1-D velocity models are for locating regional earthquakes while the Haslinger model is a 1-D local model for the Gulf of Arta (about 110 km to the North of the epicenter)

Velocity models					
Athens (NOA) model		Patras model		Haslinger model	
Depth to top of layer (km)	V_P (km/sec)	Depth to top of layer (km)	V_P (km/sec)	Depth to top of layer (km)	V_P (km/s)
0.0	5.3	0.0	5.7	<0.5	3.50
4.0	6.0	5.0	6.0	0.5–2.0	5.47
33.0	6.9	18.0	6.4	2.0–10.0	5.50
45.0	7.9	39.0	7.9	5.0–10.0	6.00
85.0	8.3			10.0–15.0	6.20
				15.0–20.0	6.48
				20.0–30.0	6.70
				30.0–40.0	6.75
				>40.0	8.00

TABLE 4 Station comparison of solution RMS (in seconds) for all 370 events. The Haslinger 1-D model performs marginally better than Patras. Station locations are shown in Fig. 3a

1-D Velocity model			
Athens	Patras	Haslinger	
Residual RMS(s) catalog data	Residual RMS(s) catalog data	Residual RMS(s) catalog data	Station
0.6022	0.6459	0.5210	ATH
0.3956	0.3834	0.3603	ITM
0.5302	0.2754	0.5152	PTL
0.1929	0.2007	0.2005	RLS
0.3512	0.3128	0.3014	VLS
0.6877	0.5921	0.5479	VLI
0.4873	0.4918	0.4848	EVR
0.5791	0.5514	0.5701	AGG
0.5453	0.4742	0.4781	LKR
0.5751	0.5514	0.5014	NAIG
0.5978	0.6124	0.6152	THL
0.6833	0.6925	0.5725	DID
0.3437	0.3484	0.3380	EFP
0.2775	0.2747	0.2783	GUR
0.5148	0.4859	0.4941	LTK
0.4995	0.4931	0.4997	PYL
0.3359	0.3431	0.3316	UPR
0.5113	0.5072	0.5081	VLX
0.4839	0.4576	0.4510	Mean RMS

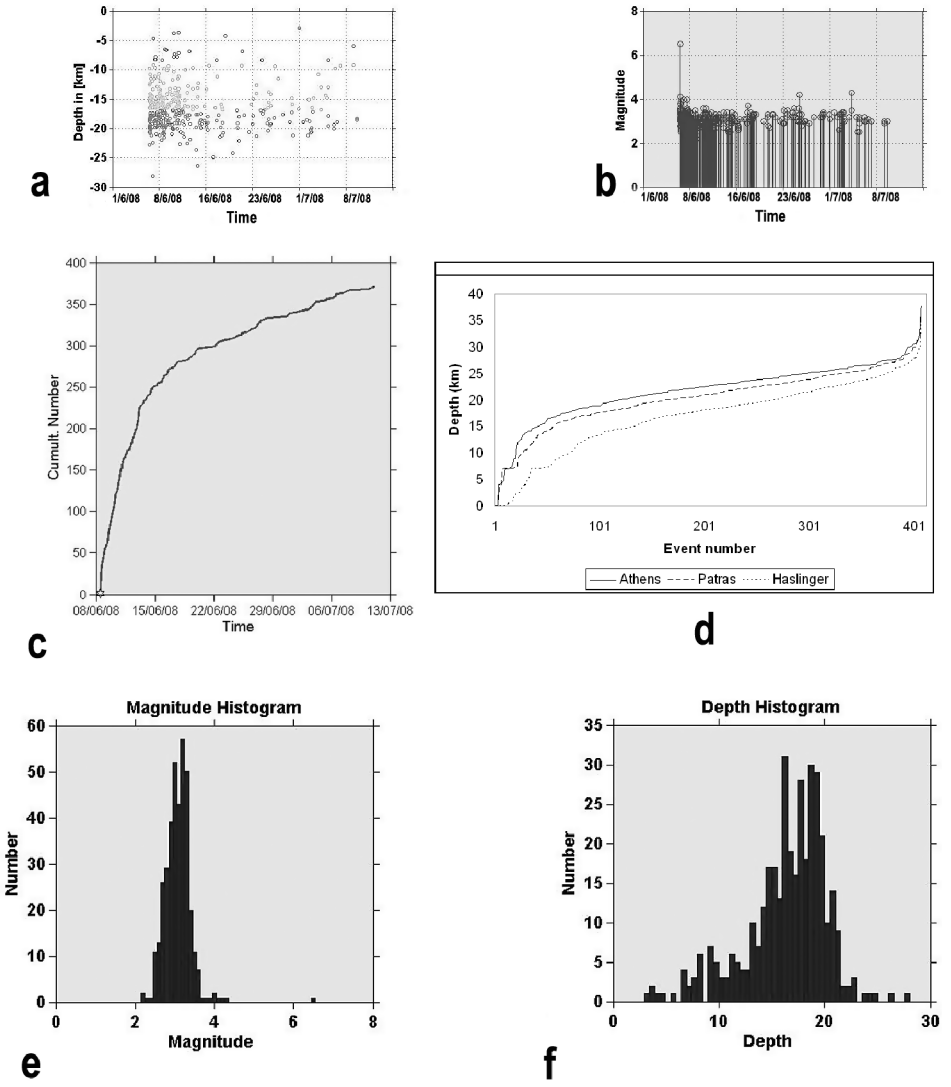

FIGURE 4 Graphs showing statistics of the aftershock sequence (370 events). (a) Depth with time, (b) M_L with time (June 8–July 8, 2008), (c) graph showing the cumulative number of events ($2.2 < M_L < 6.5$; grey line). The seismicity rate dropped drastically after June 13, 2008. (d) Cumulative graph showing comparison of relocated depths using different 1-D velocity models. The depths are sorted from shallow to deep without time or magnitude dependence. We observe that the depth difference is greater in the range 5–20 km with the Haslinger *et al.* [1999] model providing on average 4–5 km shallower depths. (e) Histogram of local magnitudes (M_L) and (f) histogram of hypocentral depths.

P-wave) = 1.0 and WTCTS (a-priori S-wave) = 0.5. This means that we gave more weights at P- phases. The method, used to solve the system of DD equations, was the conjugate gradients method (LSQR [Paige and Saunders, 1982]). 72 well-located events with $2.4 < M_L < 4.2$ during the first 24 h are shown in Fig. 2. Their alignment defines a

NE-SW striking fault plane. 370 well-located events with 2.1 < ML < 4.4 have been determined during the period June 8–July 11, 2008 (approximately one month). No seismicity shallower than 4 km was recorded. This is due to the low stress sustained at shallow crustal levels (consisting of basin fill and flysch). A statistical treatment of the June 8, 2008 sequence is presented in the following section.

3.1. Statistical Analysis of the Aftershock Sequence

Average values for the population of the 370 aftershocks include: location RMS residual = 0.27 s, azimuthal gap = 135°, horizontal error of solution = 0.9 km, vertical error of solution = 1.5 km. The azimuthal gap of 135° is due to lack of seismic stations to the SW of the epicenter (Fig. 3a). The long-axis of the aftershock sequence (first 24 h) defines a rupture zone of about 25 km in the NE-SW direction (Fig. 2a). With time, the zone of aftershocks expands mainly along strike (Fig. 2b).

Most of the 24-h aftershocks (72 events; Fig. 2a) occur (a) on the same plane that ruptured during the mainshock, (b) within 5 km from the surface projection of the rupture plane (either side), and (c) to the NE of the mainshock. It is notable the asymmetry in aftershock distribution as most aftershocks occur to the NE than to the SW of the mainshock. Strong motion data reported by Margaris *et al.* [2008] also indicate stronger motions to the NE than to the SW of the epicenter. The Kalogeras *et al.* [2008] unpublished report on the NOA web page indicates that the horizontal-PGA records from Patras (0.237 and 0.16 g; see location in Fig. 1) is almost twice the horizontal-PGA of the Pyrgos city record. Both NOA stations are located approximately 35 km away from the epicenter (Fig. 1). These observations suggest a unilateral mainshock rupture towards the NE.

The linear trend of the aftershock epicenters is also visible in the aftershock data spanning the period June 8–July 11, 2008 (approximately one month) where 370 well-located events with 2.1 < ML < 4.4 have been determined. The concentration of aftershocks near the fault plane (Fig. 2) happens because (a) of the irregular co-seismic slip distribution that leaves fault patches with increased stress and (b) static stress transfer especially at the ends of the rupture. In addition, comparing Figs. 2a and 2b it is clear that the sequence expands bilaterally with time. In the days after the mainshock, the aftershock zone also expands in the depth range 5–25 km (Fig. 4a), while the rate of aftershocks decreases with time (Fig. 4c). The rate of aftershock occurrence falls sharply after June 13, 2008 (Fig. 4c) with a linear trend. Both hypocenter magnitude (M_L) and depth histograms are unimodal with sharp peaks (Figs. 4e, 4f). The histogram of magnitudes depends on the completeness of the catalog, however, we have said before that our events are recorded on regional networks so that we have missed thousands of small earthquakes (M < 3). A time-M_L diagram shows the absence of strong aftershocks (5 < M < 6; Fig. 4b) and that the mean magnitude of the aftershocks remained stable.

We also computed the along-strike variation of the b-value of the aftershock sequence (following Wiemer and Wyss [2000] and Wiemer *et al.* [2002]; b-value is the slope of the cumulative frequency-magnitude distribution of earthquakes). The cross-section reveals asymmetric distribution of b-values (Fig. 5). The b-values are high (b > 1.8) towards the North-northeast of the rupture area and above the hypocenter while low b-value patches show up towards the SW of the hypocenter (Fig. 5) and mostly outside the rupture area. We hypothesize that the asymmetry pattern of b-value is due to the mainshock rupture directivity and detailed slip distribution, rather than inherent structural or stress heterogeneities.

The decay of aftershocks with time was analyzed in a double logarithmic diagram (Fig. 6) where the slope of the linear fit is referred to as the **p-**value (modified Omori

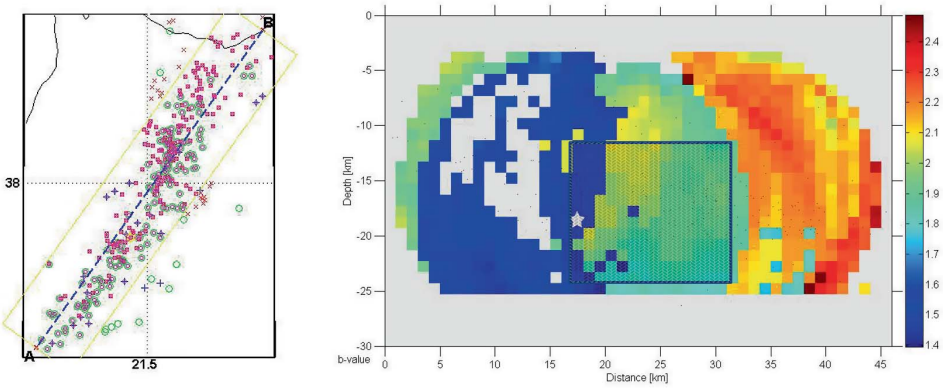

FIGURE 5 b-value variation along strike. Map on the left shows aftershock sampling volume and image on the right the b-value distribution section AB. Blue colors indicate low b-values. Low b-values are obtained mainly to the SW of the hypocentre and higher b-values both above and to the NE of the hypocenter. These variations are related to differences in rupture directivity than in pore pressure, and/or material heterogeneity. Star denotes the location of the mainshock and shaded rectangle the fault plane model (according to Table 4). (Figure available in color online.)

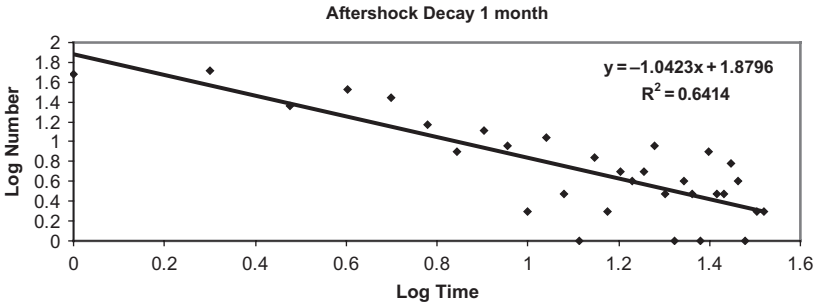

FIGURE 6 Graph showing the number of aftershocks per day plotted against the number of calendar days after the mainshock. The decay parameter p (1.04) is typical.

formula; Utsu *et al.* [1995]). In this case, **p** = 1.04 (R^2 = 0.64) for the period June 9 (t+1) until July 11 (t+32). This p-value refers to the whole aftershock sequence (370 well-located events) and it shows a typical aftershock decay rate.

4. Stress Transfer

We use a preliminary fault model provided by the NOA MT (Moment Tensor) solution (210/82/175; strike/dip/rake; Table 2) and the empirical relationship of Wells and Coppersmith [1994] for rupture length versus magnitude to constrain the rupture extent.

$$\mathbf{L} = \mathbf{10}^{-\mathbf{3.22}+\mathbf{0.69Mw}}. \tag{1}$$

Using (1) we obtain L = 15.7 km. We adopt a value of 15 km in our modeling although this estimate may be proven a bit conservative in future co-seismic slip distribution

studies of this earthquake. It is assumed that this was the length of slip patch where the strongest moment release occurred in the fault (it is possible that smaller slip patches are distributed at various depths within the total fault length). Here we need (because of the software constraints) to model elastic stress transfer using the simplest model, that of the continuous and uniform-slip rupture. Also, the rupture did not reach the surface because of the depth of the mainshock (18 km).

Then, a planar fault surface is assumed as the hosting rupture surface on which the amount and direction of slip does not change (uniform slip model with no taper). A homogeneous isotropic medium is assumed as the hosting volume of rock. Because of the rectilinear aftershock distribution and the relative location of the main shock (Fig. 2) it is reasonable to model the fault plane as extending mainly to the NE of the hypocenter. In this way, we model the sub-vertical fault plane 5 km off-centered with respect to the HypoDD hypocenter, with the following dimensions: 12 km long in the down-dip direction and 15 km long in the along-strike direction. A higher value in the down-dip direction seems unrealistic because of the depth of the mainshock; we allow for 6 km of rupture down-dip of the hypocentre which is located at 18 km depth, i.e., we stop the rupture when we reach the brittle-ductile transition at 22–24 km depth. Then, we adopt an elastic deformation model in a half-space [Okada, 1992] to compute co-seismic stress tensors within a 50 x 50 km grid from the epicenter. The observation grid is horizontal with 1 km spacing and at depths of 18 km. The calculations are performed in a Cartesian (UTM; Universal Transverse Mercator) coordinate system (x, y, z). We calculate Coulomb stress change on receiver failure planes parallel to, and with the same sense of slip as, our source model hypocentral plane; the change in Coulomb stress is given by [Reasenberg and Simpson, 1992; Stein, 1999]:

$$\mathbf{\Delta CFF} = \Delta\tau + \mu'\Delta\sigma_{\mathbf{N}}, \tag{2}$$

where $\Delta\tau$ is the coseismic change in shear stress in the direction of fault slip, $\Delta\sigma_{\mathbf{N}}$ is the change in normal stress (with tension – unclamping positive), and μ' is the effective coefficient of friction, accounting for pore-fluid pressure effects. For this work, we use $\mu' = 0.4$, an intermediate value which was found effective in describing the broad distributions of aftershocks that follow large earthquakes [Parsons *et al.*, 1999], and we perform all calculations using a Poisson's ratio of 0.25 and a shear modulus of 300,000 bar. Co-seismic displacements are computed using the M_o-Mw relationship where the seismic moment is defined as:

$$\mathbf{M_o} = \mathbf{G} \times \mathbf{L} \times \mathbf{W} \times \mathbf{D}, \tag{3}$$

in which **L** is fault length (from relation 1), **W** is fault width (12 km), **D** is average slip (the unknown), and **G** is the shear modulus, which is about 3×10^{11} dyne/cm^2. The relationship between seismic moment and magnitude is

$$\mathbf{Mw} = (\mathbf{log M_o}/\mathbf{.5}) - \mathbf{10.7}, \tag{4}$$

where $\mathbf{M_o}$ is in units of dyne-cm [Kanamori, 1978]. Combining (3) and (4) we obtain $\mathbf{u_s}$ = 0.734 m (right-lateral offset) and $\mathbf{u_d}$ = 0.064 m (upwards offset). All the modeling parameters are summarized in Table 5.

Assuming that the rupture area **RA** of the mainshock is determined by **L** = 15 km and **W** = 12 km (RA = 180 km^2) and using the formula for a circular fault [Eshelby, 1957; Kanamori and Anderson, 1975]

TABLE 5 Parameters of dislocation modeling

Epicenter Latitude - Longitude	37.940 N – 21.478 E
Grid center Latitude - Longitude	37.990 N – 21.520 E
Fault top edge UR	38.055 N – 21.556 E
Fault top edge LL	37.934 N – 21.475 E
Depth of Hypocenter	18 km
Rupture Length	15 km
Rupture Width	12 km
Strike/dip/rake	210°/82°/175°
Moment Magnitude	6.4
Strike-slip displacement (dextral)	0.734 m
Dip – slip displacement (reverse)	0.064 m
Coefficient of Friction	0.4
Shear Modulus	300000 bar
Grid size	1 km

$$\Delta\sigma = 7/16^{*}\mathbf{M_o}/\mathbf{r}^3, \tag{5}$$

where $\mathbf{M_o} = 4.49 \times 10^{25}$ (dyn cm) and $\mathbf{r} = 7.5$ km ($r \sim L/2$, RA=176.7 km^2), we obtain $\Delta\sigma = 46$ bar for the static stress drop.

Solving for receiver planes similar to the source fault we find that the mainshock transferred 1–2 bar to the neighboring fault segments on both sides of the rupture and 0.1–0.2 bar of Coulomb stress to the regions of Patras and Amalias (Fig. 7a). The clusters of off-fault aftershocks at both ends of the seismic fault have received 0.5–2 bar of Coulomb stress, encouraging their occurrence. Review studies of stress transfer [e.g., Harris, 1998; Stein, 1999] have indicated that **ΔCFF** levels exceeding 0.1 bar are associated with significant triggering of aftershocks and regional seismicity. A cross-sectional view of the Coulomb stress pattern along the main rupture shows that stress levels have increased along strike with **ΔCFF** > 3 bar at distances up to 5 km surrounding the slip model (Fig. 7b). Aftershocks occurring at a high angle to the seismic fault (Fig. 7a) are not explained by our homogeneous slip model but could be due to (a) heterogeneous slip that modifies the static stress transfer change across the fault, (b) on fluid motion in the upper crust, (c) on damage in the vicinity of the rupture (brittle microcracking), and (d) transmitted dynamic stress changes.

Our results also suggest that the SW Achaia earthquake should have advanced the time of the next earthquake on NE-SW segments, which are along-strike of the seismic fault (Fig. 7b; see Fig. 2b for the location of the inferred fault segment to the SW of the epicenter). Because those segments have a poorly known history of prior earthquakes and an unknown background stress state, we cannot estimate which of these segments is most likely to rupture next, but these two segments deserve attention as possible sources for significant future earthquakes. Other major faults in the region to the NW and to the SE of the epicenter experienced negative static Coulomb stress changes.

5. Field Observations

A NOA team visited the epicentral area twice during June 2008 (on June 15 and 21). The field work included mapping of surface effects and measurements of their attitude,

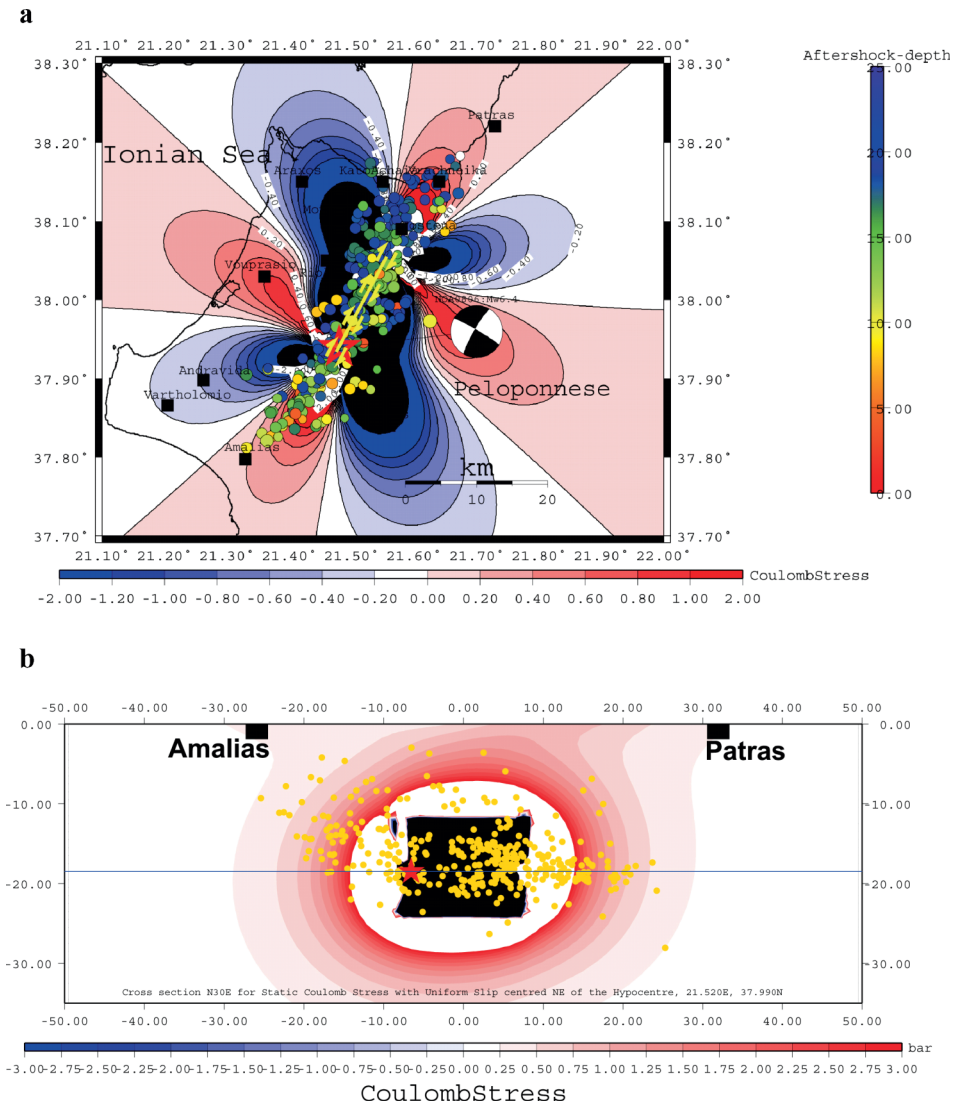

FIGURE 7 (a) Map view of Coulomb stress at 18 km depth, for receiver planes parallel to our model rupture plane (210/82/175) using a coefficient of friction of 0.4. Solid circles: Double-difference locations for earthquakes in the region of the SW Achaia earthquake. Phase picks from the NOA broadband network were used to relocate the mainshock, and 370 aftershocks (red; M_L>2.1), occurring during 8/6–11/7/2008. Red star: event hypocenter. Solid yellow line: surface projection of our model fault (b) Fault-parallel cross section of ΔCFF on our model rupture plane (N30°E). Red star: hypocenter; blue line intersection of map view plane (Fig. 5a). In both subfigures, red indicates positive ΔCFF, encouraging rupture, and blue indicates negative ΔCFF (relaxation). (Figure available in color online.)

displacements, etc. All the effects were of secondary (gravitational) origin and no primary surface ruptures were found. As noted in aftershock maps (Fig. 2) the seismic fault cuts across topography and geological formations. The ground effects were the following: (a) sand boils and liquefaction sites (Fig. 8a), (b) rock falls, (c) ground fissures (Fig. 8b),

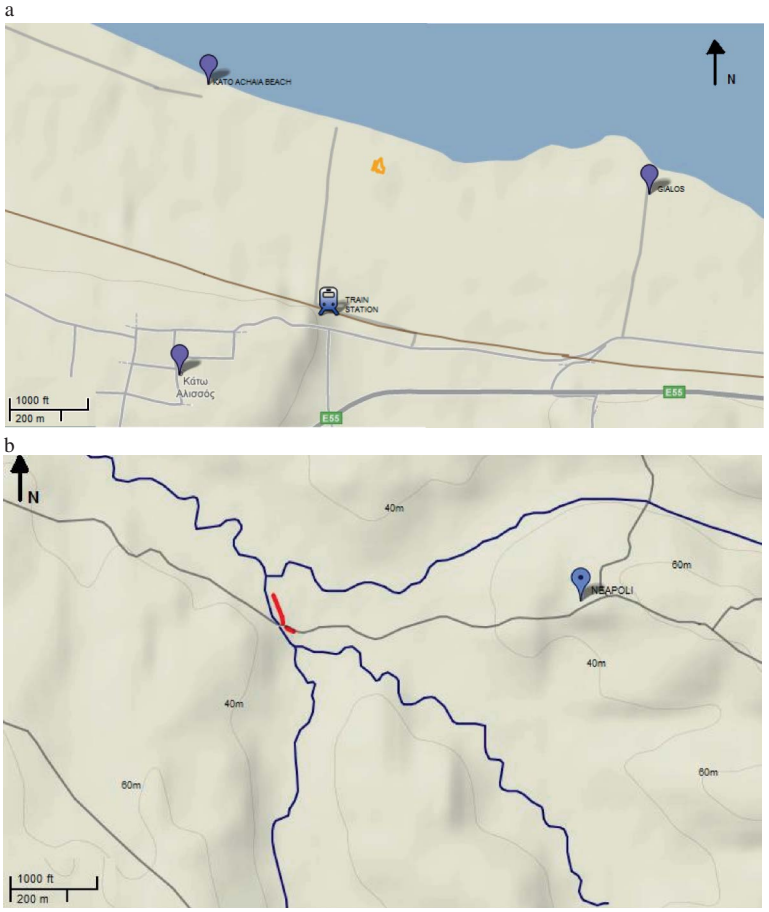

FIGURE 8 (a) Google relief image of the Kato Achaia coastal area and train station. The liquefaction site (Smertoula) is indicated by the orange polygon. The railway lines were distorted for a distance of a few hundred metres on either side of the train station. Grey lines are roads. Location with respect to the epicenter is shown on Fig. 1. (b) Google relief image of Neapolis village area showing location of NW-SE fissure (red solid line). Blue solid lines indicate streams (flow to the left). Grey lines are roads (c) field photograph of fissure in Fig. 8b showing small sinistral displacement. View to the Northeast. Figure by AG on June 21, 2008. Location with respect to the epicenter is shown on Fig. 1. (Figure available in color online.)

and (d) renewed flows in hot springs. Multiple sand boils and liquefaction ejecta were mapped in Kato Achaia beach and near Neapolis, i.e., to the N and W of the rupture (Fig. 2). The strength of ground shaking was certainly sufficient to cause liquefaction, as the local materials (alluvial and beach deposits) are susceptible and the groundwater table was near the surface. Numerous rock falls occurred in the mountainous area of mount Movri and Skolis anticline, along high-slope cliffs. Most rock falls were mapped in villages Santomeri and Portes (Fig. 2). Longitudinal surface breaks (fissures) were mapped near Neapolis and Mihoi (Fig. 2). Both fissures strike NW-SE, i.e., almost orthogonal to the seismic fault. The fissure in Mihoi is developed along a NW-striking, north-dipping cliff which attains a high slope angle. This fissure is of gravitational origin

c

FIGURE 8 (*Continued*).

and is due to strong ground shaking as it is very close to the epicenter. The Neapolis fissure (Fig. 8b) was developed inside the flat, Varda marine terrace [Stamatopoulos and Kontopoulos, 1994] along the right bank of a stream about 11 km to the NW of the epicenter. The fissure is discontinuous and comprises numerous smaller segments arranged en-echelon and dipping to the west-southwest. The amount of throw varies between 5–15 cm and a small left-lateral offset is also observed (Fig. 8c). It is possible that the fissure is the surface manifestation of a deeper, NW-SE fault plane conjugate to the mainshock fault plane. Such a plane would act as plane of weakness where gravitational effects due to passage of seismic waves could develop more easily. In the same locality we mapped a 2.4 diameter sand sprout to the east of the fissure, inside the alluvial deposits area at the right bank of river and about 300 m to the right (east) of the river (Fig. 8b). Locals informed us of more sand sprouts upstream. As a result of the earthquake the Kounoupeli hot springs were activated. Kounoupeli is an Ionian zone outcrop and its location is shown in Fig. 2.

Extensive damage to asphalt roads, railroads, and bridges was mapped in Kato Achaia town (Fig. 8a) and inside several villages within the meisoseismal area. Most structural damage occurred on old houses and constructions which signifies the good compliance of the new buildings to the antiseismic code of Greece.

6. GPS Observations

NOA has recently established a continuous GPS network in Greece [Ganas *et al.*, 2008]. All stations are equipped with Leica 1200 GRX Pro receivers and Leica AX1202 geodetic antennas. GPS signals are logged every 1 s and we sample 5 Hz (0.2 s) in the ring-buffer, as well. Currently, the on-line network comprises 10 stations at distances 10–400 km from the June 8, 2008 epicenter. For the day of June 8, 2008 we examined the records of all NOANET stations (http://www.gein.noa.gr/gps.html), however we detected no motion

other than that of station RLS (located at village Riolos to the NNW of the epicenter; Figs. 2, 3). The nearest station (other than RLS) is VLSM (island of Cephalonia) which is located 83.6 km to the WNW of the epicenter (shown onshore Cephalonia in Fig. 1). We analyzed the continuous (CGPS) GPS data following a three step approach, as described in Serpelloni *et al.* [2006]. In the first step, CGPS phase data have been analyzed by means of the GAMIT software (version 10.33; King and Herring [2008]), adopting standard procedures for regional networks [see Serpelloni *et al.*, 2006 for more details], using the IGS absolute phase center model for stations and satellites, and precise orbits from SOPAC. In the second step, we use the GLOBK software to combine our loosely constrained solutions with global and regional IGS and EUREF loosely constrained solutions provided by SOPAC (http://sopac.ucsd.edu). In this step, both orbital and common station parameters are estimated and removed for forward analysis, and only loose constraints are applied. In the third step, we define the reference frame for our velocity solution applying generalized constraints [Dong *et al.*, 1998, 2002] while estimating a seven-parameter Helmert transformation. In this step, we obtain station position time-series that are later used to fit constant velocities and additional parameters (i.e., jumps and seasonal terms). Specifically, we define the reference frame by minimizing the horizontal velocities of 50 IGS core stations with respect to the IGS00 realization of ITRF2005-NNR frame [Altamimi *et al.*, 2007]. Time series have been analyzed to determine the June 8, 2008 earthquake co-seismic jumps at stations closer to the epicenter. The uncertainties of the measurement are given as Weighted Root Mean Square errors (WRMS in Fig. 9). For example, on the N-S component the WRM S = 2.28 mm (for the whole time series). We estimate a linear trend together with annual and semi-annual seasonal terms, and the co-seismic jump at station RLS (Fig. 9). On June 8, 2008, the co-seismic displacements are 7.26 ± 0.28 mm in the North-South direction (movement towards the north) and 10.53 ± 0.85 mm in the vertical component (uplift). Both measurements (sign and magnitude) agree with the kinematics of the rupture (right-lateral strike-slip, west side up) although the error in the vertical component is larger than the N-S component. We also attribute the larger vertical offset to the larger error associated with the processing of GPS data on the vertical axis.

7. Discussion – Conclusions

7.1. Tectonic Implications

Geological data indicate extension inside the Gulf of Patras [Ferentinos *et al.*, 1985; Doutsos *et al.*, 1988; Chronis *et al.*, 1991] and in Northern Elis [Stamatopoulos and Kontopoulos, 1994]. However, seismological data from strong earthquakes indicate N70°E to N90°E (east-west) compression [Kiratzi and Louvari, 2003; Benetatos *et al.*, 2004; Kiratzi *et al.*, 2008]. The origin of the compression (shortening) is due to plate convergence offshore Zakynthos Island (Fig. 10). This region is part of the continental side of the plate boundary where the African lithosphere moves at about N5°W track with respect to stable Europe [Fernandez *et al.*, 2003] and subducts beneath the Aegean causing a regional compressional stress field. The origin of the tension (extension) is the spreading (opening) of the Aegean Plate as it advances towards the SW. So strain in the upper plate is taken by structures that are accommodating both processes. However, looking at the seismicity records it seems that most of upper-plate strain is accommodated by seismic slip on strike-slip faults. In this section, we propose a model to explain this strain partitioning. We propose that upper-plate, slip partitioning is related to the oblique differential motion of plates towards the end of the Hellenic Arc. In the western Hellenic

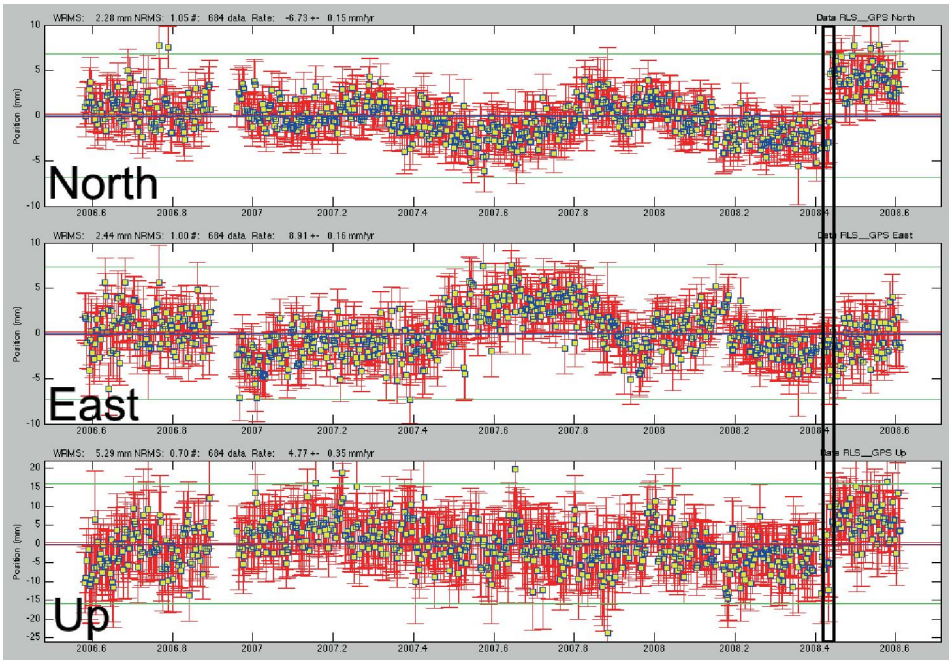

FIGURE 9 Time series of crustal deformation at GPS station RLS (North, East and Up; from top to bottom). RLS is located at 38 03′ 21.00536″ N, 21 27′ 53.07259″ E (ellipsoidal height is 132.89 m). Daily position uncertainties are indicated by the error bars. Date of earthquake is shown by vertical rectangle. Evident jump in north and up component indicates co-seismic displacements associated with the 2008 K. Achaia, Greece earthquake. The co-seismic displacement in the North-South component is 7 mm. The co-seismic displacement in the vertical component is 10 mm (uplift). (Figure available in color online.)

Arc the Nubia (Africa) plate vector moves towards N5°W (or N175°E; Fig. 10) while the upper (Aegean) plate moves toward N224°E-N242°E (points LKTR and LAKA, Fig. 10; Hollestein *et al.* [2008]), resulting in a highly oblique subduction geometry (49–67° vector divergence). This results in the formation of upper-plate faults along both arc-parallel and arc-normal directions. In Fig. 10, we point to a pattern of strike-slip tectonics including an arc-parallel structure (offshore Kyllene) which is an active sinistral fault and strikes parallel to the reverse fault (subduction interface). Similar sinistral faults occur inside the Gulf of Patras and near lake Trichonis [Kiratzi *et al.*, 2008]. On the other hand, the dextral shear emerges from the differential motion of crustal blocks in western Greece from North to South (see GPS velocity vectors in Fig. 10). As an example consider either side of the Gulf of Patras, where the velocities towards the SW increase by 50% (20 mm/yr to the North vs. 30 mm/yr to the South). This velocity contrast results in dextral shear between the two blocks as the reference frame (stable Europe) remains the same. In addition, a recent geodetic study by Hollenstein *et al.* [2008] shows a significant arc-parallel component of motion in Zakynthos and Cephalonia. This strain may be accommodated by sinistral strike-slip and minor normal faulting inside the central Ionian Sea.

A similar situation occurs in central Aegean [Ganas *et al.*, 2005] which is a different geodynamic setting. There east-west compression is accompanied by normal faulting because of the rotation of the maximum principal stress axis while least principal stress

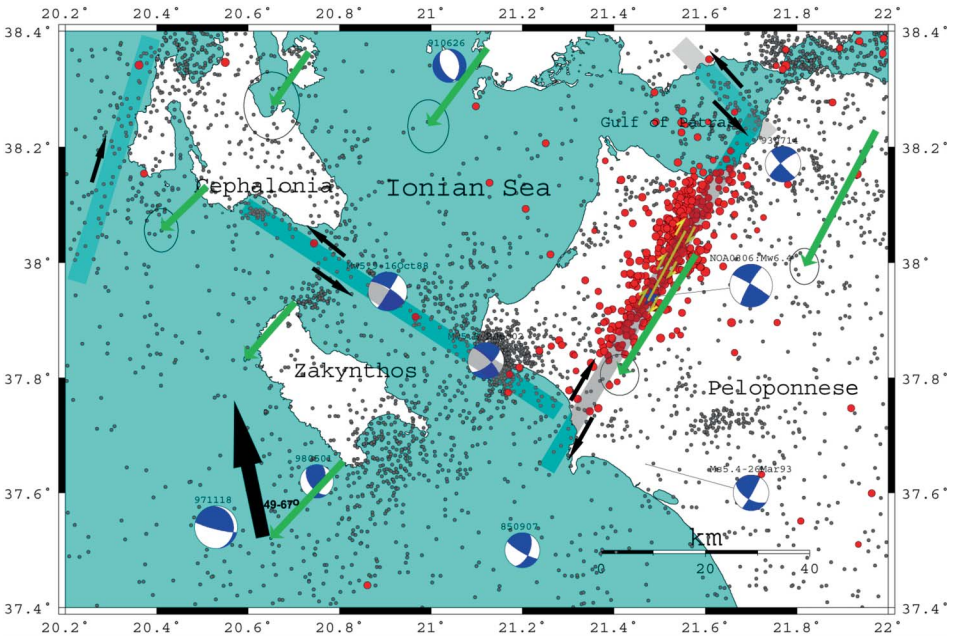

FIGURE 10 Map of western Greece showing shallow seismicity and major strike-slip fault zones (in gray shades). Gray dots: 2000–2005 earthquakes from [Roumelioti *et al*., 2007]. Red dots: June 8–July 8, 2008 earthquakes (this study). Green arrows represent GPS velocity vectors from [Hollestein *et al*., 2008]. Large, black arrow indicate the direction of motion of the Nubia (Africa) plate from Fernandes *et al*. [2003]. Small, black arrows indicate sense of slip along active, strike-slip faults. Beachballs represent lower hemisphere projections of focal planes of important events (1988–2008). Compressional quadrants are filled in blue. Yellow line with arrows indicates surface projection of the SW Achaia seismic fault. (Figure available in color online.)

(sigma min) remains horizontal at N7°-N14°E. In addition, the seismic fault of SW Achaia is comparable to the 2001 Skyros earthquake fault in terms of length and tectonic significance [Ganas *et al.*, 2005] because mean (Quaternary) slip rates of active faults in western Greece are comparable to those of central Greece (0.1– 0.5 mm/year), i.e., it is a 1–1.5 Ma old structure that controls strain accumulation in this area. We conclude that the June 8, 2008 fault is part of a large, transcurrent fault zone striking NE-SW that deforms the Aegean upper plate above the African plate subduction (Fig. 10). The activation of major NE-SW vertical structures indicate that such faults are not transfer-type faults linking normal faults inside rifts such as in the model of Flotte *et al.* [2005]. On the contrary, the strike-slip faults are the main structures and the normal faults are the minor, at the NW Peloponnese - Gulf of Patras area.

Furthermore, the SW-Achaia right-lateral shear zone may end offshore Vartholomio area (Figs. 1,10) where the NW-SE strike-slip fault of the 2002 earthquake was activated [Roumelioti *et al.*, 2004]. Seismicity relocation [Roumelioti *et al.*, 2007] indicates that the latter fault zone extends further north up to the SE shores of Cephalonia Island. The 1993 event near Patras also occurred along a strike-slip fault [Tselentis *et al.*, 1994; Kiratzi and Louvari, 2003] as well as the 1975 and 2007 seismic swarm near Lake Trichonis [Kiratzi *et al.*, 2008]. Further south, left-lateral strike-slip kinematics is reported for the 1993 earthquake near Pyrgos [Melis *et al.*, 1994]. So, the E-W normal

faults that created the Patras rift are not inactive; however, when evaluating the relative importance of structures taking up the deformation we point out that the most active ones are the strike-slip zones striking NE-SW and NW-SE. In summary, the active tectonics of NW-Peloponnese is dominated by a series of 10–20 km long strike-slip faults that are arranged in NW-SE and NE-SW directions and are active for a period of 1–1.5 Ma.

7.2. Relation and Origin of Uplift

In this section we evaluate the uplift due to co-seismic slip during 2008-type earthquakes and compare to the geological record in Northern Elis and SW Achaia [Stamatopoulos *et al.*, 1988]. The 2008 seismic fault dips steeply to the NW so it may be possible that fault-normal shortening will result on coastal uplift and formation of a flight of marine terraces. For this purpose, a dislocation model similar to the slip model used for stress transfer modeling (Fig. 7) is built and deformation is computed in an elastic half-space. First, the surface deformation due to slip on a sub-vertical strike slip fault is computed. For type-2008 ruptures the static displacement per event is 0.02–0.03 m (3 cm; dip-slip component) in the region near Neapolis (Figs. 2 and 8b) so we estimate that between 660–1000 events with M > 6 are necessary to raise the isotope stage 5e marine terrace to the present day elevation of 20 m above mean sea level. Given this dislocation model the average recurrence time is calculated to be 120–180 years as the age of the terrace is 120,000 years (Tyrrhenian; Stamatopoulos *et al.* [1988]). We conclude that this scenario overestimates the seismicity rate in this area by a factor of 10.

Another cause of regional uplift in this area of Greece could be the existence of viscous evaporates, that may be associated with surface uplift during large, thrust-fault earthquakes. Evaporites exist at the base of the Ionian zone in western Greece and have been mobilized during thrusting from east-to-west in Miocene-Pliocene times [Underhill, 1988]. However, the vast portion of active seismicity we record today in western Greece is located in greater depths (> 4–7 km) that is regarded as the depth of the evaporitic decollements so there is no reason to consider those structures as active today. In addition, continuous GPS results from Cephalonia and Zakynthos stations [Hollenstein *et al.*, 2008] point to interseismic subsidence (with respect to stable Europe).

Above considerations show that regional uplift is due to another process and not to earthquakes. The most likely cause is upper plate deformation (flexure) due to plate convergence [Ganas and Parsons, 2009]. The overriding plate motion towards the South Ionia Sea trench ranges from 20–32 mm/yr (Fig. 10), seismic coupling is high [Laigle *et al.*, 2004] so continental plate topography is created due to the frictional resistance of the plate interface [Hampel and Pfiffner, 2006]. The small amount of Quaternary uplift in comparison to other region of the Hellenic Arc (e.g., Crete) is due to highly oblique convergence in the area of NW Peloponnese.

8. Conclusions

(a) The hypocenter of the June 8, 2008 Mw = 6.4 event was determined at 18 km depth beneath village Mihoi in SW Achaia.
(b) No surface rupture was observed.
(c) Many rock falls, slides, and liquefaction features have been found as is typical for an earthquake of this size.
(d) Double-difference relocations of 370 aftershocks show a linear pattern of events and define a clear NE-SW striking mainshock fault plane (Fig. 2).

(e) The 24-h aftershock region extends nearly 25 km in length, and the width of the surface projection of the aftershocks ranges between 5–10 km. The depth of the aftershocks rarely exceeds 22 km.
(f) Modeling of the stress changes shows a large (about 1–3 bar; Fig. 7) stress change on neighboring faults towards the towns of Patras and Amalias, encouraging right-lateral slip.
(g) GPS data from the NOANET GPS Network (station RLS; Fig. 9) have been analyzed to obtain measurements of the static displacement field associated with the earthquake. An amount of 7 mm of co-seismic offset to the North was recorded in agreement with the right-lateral kinematics of the source.
(h) The regional uplift is not due to co-seismic slip along the SW Achaia fault. This is clear from dislocation modeling. It is due to the overriding plate motion towards the trench and the frictional resistance of the plate interface [Hampel and Pfiffner, 2006; Ganas and Parsons, 2009].
(i) We develop a qualitative model of the deformation in NW Peloponnese within the regional setting of Africa-Eurasia convergence (Fig. 10). Our model favors slip partitioning along normal and strike-slip faults on the upper (Aegean) plate. Normal faults are less active than strike-slip faults.
(j) The active tectonics of western Greece is dominated by a series of 10–20 km long strike-slip faults that are arranged in NW-SE and NE-SW directions and are active for a period of 1–1.5 Ma

Acknowledgments

We thank many colleagues at the Institute of Geodynamics who have maintained the operation of continuous GPS stations and participated in the field work in Kato Achaia during June 2008 and especially Nikos Melis, Sofia Rontogianni, Panagiota Petrou, Panayiotis Argyrakis, Ifigeneia Boutsi, and Kostas Boukouras. We also thank the local witnesses Petros Mourtikas and Antonis Kastanas for their help on the field. We are indebted to George Stavrakakis, Spiros Pavlides, Efthimos Sokos, and Leonidas Stamatopoulos for comments and suggestions. We thank Evangelos Lagios for making available the Leica receiver in station RLS. We used Bob Simpson's DLC code for our stress transfer modeling, and we thank Bob for his help. We plotted some figures using the Generic Mapping Tools (GMT) software. This research was financed by GSRT (http://www.gsrt.gr) and EU project PREVIEW. 30 s data from NOA GPS stations can be downloaded from: http://www.gein.noa.gr/gps.html

References

Ambraseys, N. N. and Jackson, J. A. [1997] "Seismicity and strain in the Gulf of Corinth (Greece) since 1694," *Journal of Earthquake Engineering* **1**(3), 433–474.

Benetatos, C., Kiratzi A., Papazachos C., and Karakaisis G. [2004] "Focal mechanisms of shallow and intermediate depth earthquakes along the Hellenic Arc," *Journal of Geodynamics* **37**, 253–296.

Chronis, G., Piper, D. J. W., and Anagnostou, C. [1991] "Late Quaternary evolution of the Gulf of Patras, Greece: Tectonism, deltaic sedimentation and sea-level change," *Marine Geology* **97**, 191–209.

Dong, D., Herring, T. A., and King, R. W. [1998] "Estimating regional deformation from a combination of space and terrestrial geodetic data," *Journal of Geodynamics* **72**, 200–214.

Dong, D., Fang, P., Bock, Y., Cheng, M. K., and Miyazaki, S. [2002] "Anatomy of apparent seasonal variation from GPS-derived site position," *Journal of Geophysical Research* **107** (B4).

Doutsos, T., Kontopoulos, D., and Frydas, D. [1987] "Neotectonic evolution of northwestern continental Greece," *Geological Research* **76**(2), 433–450.

Doutsos, T., Kontopoulos N., and Poulimenos G. [1988] "The Corinth-Patras rift as the initial stage of continental fragmentation behind an active island arc (Greece)," *Basin Research* **1**, 177–190.

Eshelby, J. D. [1957] "The determination of the elastic field of an ellipsoidal inclusion, and related problems," *Proc. of the Royal Society of London A* **241**, 376–396.

Ferentinos, G., Brooks, M., and Doutsos, T. [1985] "Quaternary tectonics in the Gulf of Patras, western Greece," *Journal of Structural Geology* **7**(6), 713–717.

Fernandes, R. M. S., Ambrosius, B. A. C., Noomen, R., Bastos, L., Wortel, M. J. R., Spakman, W., and Govers R. [2003] "The relative motion between Africa and Eurasia as derived from ITRF2000 and GPS data," *Geophysical Ressearch Letters* **30**(16), 1828.

Flotte, N., Sorel, D., Muller, C., and Tensi, J. [2005] "Along strike changes in the structural evolution over a brittle detachment fault: example of the Pleistocene Corinth–Patras rift (Greece)," *Tectonophysics* **403**(1–4), 77–94.

Galanopoulos, G. A. [1981] "The damaging shocks and the earthquake potential of Greece," *Annales Geologiques des Pays Helleniques* **30**, 648–724.

Ganas, A., Drakatos, G., Rontogianni, S., Tsimi, C., Petrou, P., Papanikolaou, M., Argyrakis, P., Boukouras, K., Melis, N., and Stavrakakis, G. [2008] "NOANET: the new permanent GPS network for Geodynamics in Greece," *Geophysical Research Abstracts* **10**, EGU2008-A-04380.

Ganas, A., Drakatos, G., Pavlides, S. B., Stavrakakis, G. N., Ziazia, M., Sokos, E., and Karastathis, V. K. [2005] "The 2001 Mw = 6.4 Skyros earthquake, conjugate strike-slip faulting and spatial variation in stress within the central Aegean Sea," *Journal of Geodynamics* **39**, 61–77.

Ganas, A. and Parsons, T. [2009] "Three-dimensional model of Hellenic Arc deformation and origin of the Cretan uplift," *Journal of Geophysical Research* **114**, (B06404).

Hampel, A. and Pfiffner, A. [2006] "Relative importance of trenchward upper plate motion and friction along the plate interface for the topographic evolution of subduction-related mountain belts," *Geological Society, London, Special Publications* **253**, 105–115.

Harris, R. A. [1998] "Introduction to special section: Stress triggers, stress shadows, and implications for seismic hazard," *Journal of Geophysical Research* **103**(24), 347–358.

Haslinger F., Kissling E., Ansorge J., Hatzfeld, D., Papadimitriou, E., Karakostas, V., Makropoulos, K., Kahle, H.-G., and Peter, Y. [1999] "3D crustal structure from local earthquake tomography around the Gulf of Arta (Ionian region, NW Greece)," *Tectonophysics* **304**(3), 201–218.

Hatzfeld, D., Pedotti, G., Hatzidimitriou, P., and Makropoulos, K. [1990] "The strain pattern in the western Hellenic arc deduced from a microearthquake survey," *Geophysical Journal International* **101**, 181–202.

Herring, T. A. King, R. W., and McClusky, S. C. [2006] *Documentation for GAMIT GPS Analysis Software*, version 10.3, Massachusetts Institute of Technology and Scripps Institution of Oceanography.

Hollenstein, C., Müller, M. D., Geiger, A., and Kahle, H. G. [2008] "Crustal motion and deformation in Greece from a decade of GPS measurements, 1993–2003," *Tectonophysics* **449**, 17–40.

Kalogeras, I., Loukatos, D., and Stavrakakis, G. [2008] "Preliminary report for the strong motion data of the 8 June 2008 Earthquake (Mw 6.4) in Achaia - Elia, Western Greece," available from http://www.gein.noa.gr/services/achaia/sm_table.htm (accessed March 13, 2009).

Kamberis, E., Ioakim, C. H., Tsaila-Monopolis, S. T., and Tsapralis V. [1992] "Geodynamic and palaeogeographic evolution of western Peloponnese (Greece) during the Neogene," *Paleontologia I Evolucio* **24–25**, 363–376.

Kanamori, H. and Anderson, D. L. [1975] "Theoretical basis of some empirical relations in seismology," *Bulletin of the Seismological Society of America* **65**(5), 1073–1095.

Kanamori, H. [1978] "Quantification of earthquakes," *Nature* **271**, 411–414.

Kiratzi, A. and Louvari, E., [2003] "Focal mechanisms of shallow earthquakes in the Aegean Sea and the surrounding lands determined by waveform modeling: a new database," *Journal of Geodynamics* **36**, 251–274.

Kiratzi, A., Sokos, E., Ganas, A., Tselentis, A., Benetatos, C., Roumelioti, Z., Serpetsidaki, A., Andrianopoulos, G., Galanis, O., and Petrou, P. [2008] "The April 2007 earthquake swarm near Lake Trichonis and implications for active tectonics in western Greece," *Tectonophysics* **452**(1), 51–65.

Laigle, M., Sachpazi, M., and Hirn, A. [2004] "Variation of seismic coupling with slab detachment and upper plate structure along the western Hellenic subduction zone," *Tectonophysics* **391**, 85–95

Lekkas, E., Logos, E., Danamos, G., Fountoulis, I., and Adamopoulou, E. [1991] "Macroseismic observations after the earthquake of October 16th, 1988 in Kyllini peninsula," *Bulletin of the Geological Society of Greece* **25**(3), 313–328.

Margaris et al. [2008] Preliminary report on the principal seismological and engineering aspects of the Mw = 6.5 Achaia-Ilia (Greece) earthquake on 8 June 2008, available from http://research.eerc.berkeley.edu/projects/GEER/GEER_Post%20EQ%20Reports/Greece_2008/greece_2008_index.html (accessed March 13, 2009).

Melis, N. S. and Konstantinou, K. I. [2006]. "Real-time seismic monitoring in the Greek region: an example from the 17 October 2005 east Aegean Sea earthquake sequence," *Seismological Research Letters* **77**(3), 364–370.

Melis, N., Tselentis, G., and Sokos, E. [1994] "The Pyrgos (March 26, 1993; Ms=5.2) earthquake sequence as it was recorded by the Patras seismic network," *Bulletin of the Geological Society of Greece* **30**(5), 175–180.

Okada, Y. [1992] "Internal deformation due to shear and tensile faults in a halfspace," *Bulletin of the Seismological Society of America* **82**, 1018–1040.

Parsons, P., Stein, R. S., Simpson, R. W., and Reasenberg., P. A. [1999] "Stress sensitivity of fault seismicity: A comparison between limited-offset oblique and major strike-slip faults," *Journal of Geophysical Research* **104**(B9), 20183–20202.

Reasenberg, P. A. and Simpson, R. W. [1992] "Response of regional seismicity to the static stress change produced by the Loma Prieta earthquake," *Science* **255**, 1687–1690.

Roumelioti, Z., Ganas, A., Sokos, E., Petrou, P., Serpetsidaki, A., and Drakatos, G. [2007] "Toward a joint catalogue of recent seismicity in western Greece: preliminary results," *Bulletin of the Geological Society of Greece* **40**, 1257–1266.

Roumelioti, Z., Benetatos, C., Kiratzi, A., Stavrakakis, G., and Melis, N. [2004]. "A study of the 2 December 2002 (M5.5) Vartholomio (western Peloponnese, Greece) earthquake and of its largest aftershocks," *Tectonophysics* **387**(1–4), 65–79.

Sachpazi, M., Galvé, A., Laigle, M., Hirn, A., Sokos, E., Serpetsidaki, A., Marthelot, J. M., Alperin, J. M. Pi, Zelt, B., and Taylor, B. [2007] "Moho topography under central Greece and its compensation by Pn time-terms for the accurate location of hypocenters: The example of the Gulf of Corinth 1995 Aigion earthquake," *Tectonophysics* **440**, 53–65.

Serpelloni, E., Casula, G., Galvani, A., Anzidei, M., and Baldi, P. [2006] "Data analysis of permanent GPS networks in Italy and surrounding regions: application of a distributed processing approach," *Annals of Geophysics* **49**(4–5), 1073–1104.

Stamatopoulos, L., Belluomini, G., Branca, M., Manfra, L., and Voltaggio, M. [1988] "230Th/234U and isoleucine epimerization dating of Quaternary marine deposits in western Peloponnese (Greece)," *Z. Geomorph. N. F.* **42**(2), 245–253.

Stamatopoulos, L. and Kontopoulos, N. [1994] "Geomorphology and evolution of the region between Lapa and Eleotopos, northwestern Peloponnese (Greece)," *Il Quaternario* **7**(2), 537–544.

Stein, R. S. [1999] "The role of stress transfer in earthquake occurrence," *Nature* **402**, 605–609.

Tselentis, G., Melis, N., and Sokos, E. [1994] "The Patras (July 14, 1993; Ms=5.4) earthquake sequence," *Bulletin of the Geological Society of Greece* **30**(5), 159–165.

Underhill, J. [1988] "Triassic evaporites and Plio-Quaternary diapirism in western Greece," *Journal of the Geological Society* **145**, 269–282.

Utsu, T., Ogata, Y., and Matsu'ura, R. S. [1995] "The centenary of the Omori formula for a decay law of aftershock activity," *Journal of Physical Earth* **43**, 1–33.

Waldhauser, F. [2001] ‘‘hypoDD – A program to compute double-difference hypocenter locations,’’ *U.S. Geological Survey Open-File Report*, 01–113.

Waldhauser, F. and William L. E. [2000] ‘‘A double-difference earthquake location algorithm: Method and application to the northern Hayward fault, California,’’ *Bulletin of the Seismological Society of America* **90**, 1353–1368.

Wells, D. G. and Coppersmith, K. J. [1994] ‘‘New empirical relationships among magnitude, rupture length, rupture width, rupture area, and surface displacement,’’ *Bulletin of the Seismological Society of America* **84**, 974–1002.

Wiemer, S. and Wyss M. [2000] ‘‘Minimum magnitude of complete reporting in earthquake catalogs: Examples from Alaska, the Western United States, and Japan,’’ *Bulletin of the Seismological Society of America* **90**, 859–869.

Wiemer, S. Gerstenberger, M., and Hauksson, E. [2002] ‘‘Properties of the aftershock sequence of the 1999 Mw 7.1 Hector Mine earthquake: implications for aftershock hazard,’’ *Bulletin of the Seismological Society of America* **92**, 1227–1240.